

Photodissociative excitation processes of XeF₂ in the vacuum ultraviolet region 105–180 nm

Mitsuhiko Kono and Kosuke Shobatake^{a)}

Department of Functional Molecular Science, The Graduate University for Advanced Studies, and Institute for Molecular Science, Myodaiji, Okazaki 444, Japan

(Received 21 November 1994; accepted 13 January 1995)

Photodissociative excitation processes of XeF₂ are studied by absorption and photofragment fluorescence spectroscopies in the vacuum UV region 105–180 nm. The quantum yields are measured along with the dispersed fluorescence spectra for emissions from XeF* (*B*, *C*, and *D*) excimers formed from XeF₂ excited by linearly polarized, monochromatized synchrotron radiation. Fluorescence anisotropy, *R*, of XeF* fragment emission was also measured against excitation light wavelength in the region 105–165 nm. The quantum yields for XeF* excimer formation are found to be very high; especially in the valence band region shorter than 130 nm it reaches almost unity. From the fluorescence measurements we have observed new peaks assigned to 5π_u→5dR Rydberg transitions. The intense 5π_{u3/2}→6sR bands which appear around 143 nm exhibit no fluorescence excitation bands; even fluorescence dips are observed at 143.18 and 144.25 nm whereas very weak positive fluorescence bands are observed at 141.04 and 142.11 nm. The *R* values for the very broad valence bands which underlie intense Rydberg bands are found to be high. The 5π_u series of Rydberg bands exhibit low *R* values. Based on the energetics and the results of quantum yields and fluorescence anisotropy values, the valence and Rydberg bands observed are assigned from the viewpoint of symmetry of the excited state, and the dynamics of the dissociation processes is discussed. © 1995 American Institute of Physics.

I. INTRODUCTION

Since the discovery of the first noble-gas compounds in 1962, XeF₂ has attracted great attention and its chemical activity, electronic and geometric properties have been investigated experimentally and theoretically because of its simple structure with *D_{∞h}* symmetry and unique electronic properties.^{1–17} From the photochemical point of view it is a special molecule since strong XeF* excimer emission has been detected in photolysis in the vacuum UV region.

The dispersed fluorescence spectra for XeF* formed in the photolysis of XeF₂ with Kr, Hg, and CO resonance radiation² and ArF excimer laser³ have been observed by Brashears, Setser, and Desmarteau, and by Bott *et al.*, respectively. Bibinov and Vinogradov have estimated the quantum yields for total XeF* excimer emission as about 0.34 in the region of continuum absorption⁴ (140–180 nm) and to be larger than 0.70 at 116 nm,⁵ respectively. Black *et al.* have reported the quantum yields for excimer emission as about 90% at 145 and 172 nm.⁶ Nielsen and Schwarz have made detailed assignments of the absorption bands for XeF₂ they observed in the vacuum UV region.⁷

In the present report we study the photodissociative excitation processes of gaseous XeF₂ in the excitation wavelength, λ_{ex}, region from 105 (11.8 eV) to 180 nm (6.9 eV) applying various fluorescence spectroscopic techniques for the XeF* emissions along with absorption spectroscopy using monochromatized synchrotron radiation (SR). We have measured fluorescence excitation spectra for formation of XeF* (*B*, *C*, and *D*) excimers. From the quantitative cross

sections for photoabsorption, σ_{abs}, and photoemission, σ_{em}, the quantum yields for excimer formation have been determined for the first time in the wide wavelength region of λ_{ex}=105–180 nm. We have also observed the dispersed fluorescence spectra of XeF* formed at several excitation energies to obtain rough information on the branching fractions for forming XeF* excimers in the *B*, *C*, and *D* states.

Another important technique applied in this report is the measurement of the XeF* fluorescence anisotropy defined as

$$R = \frac{I_{\parallel} - I_{\perp}}{I_{\parallel} + 2I_{\perp}}, \quad (1)$$

where *I*_∥ and *I*_⊥ are the intensities of polarized emissions parallel and perpendicular, respectively, to the electric vector of the incident light. The scalar information such as absorption and fluorescence excitation spectra alone does not provide us with enough dynamical information on photodissociation let alone the symmetry of the excited state. Measurement of fluorescence anisotropy however provides us vectorial information on photodissociative excitation processes since it reflects the nature of spatial distribution of the angular momenta of the excited fragments formed and thus the dynamics of dissociation, and the symmetry of the excited state as well as the lifetime of the excited molecule.^{18,19} Considering the fact that the XeF₂ molecule may be the system which provides the highest quantum yield for excited fragment formation, the information on the fluorescence anisotropy is expected to play a crucial role in the assignment of the excited states. This technique, originally developed by Chamberlain and Simons,^{20,21} has been applied to several triatomic or polyatomic systems, for example, OH* from H₂O (Refs. 20 and 22) or H₂O₂ (Ref. 18) and CN* from XCN [X=H (Refs. 21 and 23), Cl (Refs. 24 and 25), Br

^{a)}Present address: Department of Materials Chemistry, School of Engineering, Nagoya University, Furo-cho, Chikusa-ku, Nagoya, 464-01, Japan.

(Refs. 21, 24, and 26), and CH₃ (Ref. 27)]. Study of photo-fragment fluorescence anisotropy of the XeF₂ system has also been performed by Loge and Wiesenfeld using laser induced one-⁸ or two-photon⁹ dissociation spectroscopy. In the present study, we have determined fragment XeF* fluorescence anisotropy as a function of the λ_{ex} in the range of 105–180 nm. We attempt to resolve some of the problems associated with the symmetry and assignments of the excited states and the nature of the complicated potential energy surfaces leading to dissociation of photoexcited XeF₂, based on the information on the anisotropy of polarized fluorescence and the electronic and vibrational distributions of the XeF* excimers obtained from the dispersed fluorescence spectra at some exciting wavelengths.

II. EXPERIMENT

A. General

Absorption and fluorescence excitation spectra are observed using an apparatus for studying gas phase photochemistry which was constructed on the beam line BL2A of the Ultraviolet Synchrotron Orbital Radiation facility (UVSOR) at Institute for Molecular Science (IMS). The apparatus used is described in the previous publications.^{26,28} In brief the focused dispersed radiation from a 1 m Seya–Namioka monochromator enters a photoabsorption gas cell (with a pass length of 12.3 cm) through a LiF window. The transmitted photons are detected by a photomultiplier tube (PMT) after conversion to UV and visible light by means of a light converter, i.e., a sodium salicylate coating on the outer side of the exit LiF window. The fluorescence excitation spectrum of total emission ($B \rightarrow X$, $C \rightarrow A$, and $D \rightarrow X$) has been measured by detecting the fluorescence photons emitted and focused in the direction perpendicular to the light beam with a PMT (Hamamatsu R585) without any filter. Although the spectrum is not shown in this article, a fluorescence excitation spectrum due to XeF($B \rightarrow X$) emission was also observed using an interference filter (KL-35 Toshiba) with a maximum transmittance of 15% at 348.5 nm and a full width at half maximum (FWHM) of 20.5 nm placed in front of the PMT. The spectra for the total and partial emissions are simultaneously measured with the two-photon counting systems. The resolution of exciting light wavelength, $\Delta\lambda_{\text{ex}}$, for the measurement of absorption and fluorescence excitation spectra was 0.10 nm except for the cases specified.

The dispersed fluorescence spectra were recorded using a 32 cm monochromator (Jobin Yvon HR-320) blazed at 250 nm with a resolution of the observed emission at $\Delta\lambda_{\text{obs}}=1.2$ nm with a rather low resolution of the exciting light wavelength at $\Delta\lambda_{\text{ex}}=1.0$ nm in order to attain a high enough signal-to-noise ratio. The total photoemission cross section, σ_{em} , has been determined by comparing the excimer fluorescence intensity with that for OH($A \rightarrow X$) formed in photodissociative excitation of H₂O at 133.57 nm light whose cross section has been determined as $\sigma_{\text{em}}=0.29$ Mb (10^{-18} cm²).²⁹

The solid XeF₂ sample purchased from PCR Inc. was used as delivered. The pressure of gaseous XeF₂ was controlled by an MKS Baratron manometer at 50 mTorr.

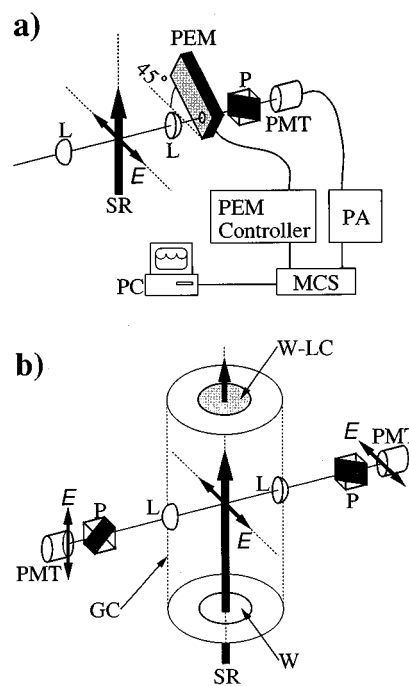


FIG. 1. Schematics of an apparatus used for photofragment polarization measurement: (a) system for absolute fluorescence anisotropy measurement (PEM-MCS system), (b) experimental setup to determine the relative ratio of the polarized fluorescence intensity parallel to that perpendicular to electric vector, E , of the incident SR light in a wide wavelength range. GC: gas cell, L: lens, MCS: multichannel scaler, P: polarizer, PA: pulse amplifier, PC: personal computer, PEM: photoelastic modulator, PMT: photomultiplier tube, SR: synchrotron radiation, W:LiF window, W-LC: light converter (sodium salicylate) coating on the outer side of the LiF window.

B. Fluorescence anisotropy measurements

The setup used to measure fragment fluorescence anisotropy, R , values on the beamline UVSOR-BL2A is essentially the same as reported previously.²⁶ Figure 1 illustrates the schematics of the system for this measurement which comprises (1) linearly polarized light from the SR source, (2) a photoelastic modulator (PEM, Hinds International Inc. PEM-80 Model CF5) followed by a calcite polarizer and a photomultiplier tube (PMT, Hamamatsu R585), and (3) a homemade multichannel scaler (MCS). The radially emitted photons are made into a parallel beam which propagates to the direction perpendicular to the electric vector and the propagation direction of the exciting light using a lens with a focal length of 25 mm and then the beam goes through the first aperture 10 mm in diameter. The parallel beam through the second aperture 10 mm in diameter was again focused with a lens with a focal length of 25 mm onto the entrance to the PMT. In order to determine absolute R values in a wide wavelength range at many frequency points within a limited measurement time, two methods have been applied, i.e., (i) a point-by-point determination of the absolute R value [see Fig. 1(a)] and (ii) the measurement of relative fluorescence intensities using two sets of calcite polarizer-photomultiplier detectors which we call a dual-detector system [see Fig. 1(b)]. The former method determines the absolute R values at a few exciting wavelengths and the latter determines the relative intensities for the polarized emissions parallel and

perpendicular to the electric vector of the exciting light, a scaling factor of which is estimated by scaling the relative values to the absolute ones determined by the former technique.

1. Determination of absolute fluorescence anisotropy using a PEM-MCS system

The system used to determine absolute fluorescence anisotropy at a few exciting light wavelengths may be called a PEM-MCS technique. The merit of using this system is that by fast modulation of a polarization rotator at a frequency of 50 kHz one can remove the factors giving rise to uneven signal levels of polarized fluorescence intensities parallel and perpendicular to the electric vector of the exciting light when a polarizer is physically rotated, such as time variation of the sample gas pressure and the difference between the detection efficiencies of the PMT for the parallel and perpendicular positions of the calcite polarizer. The fluorescence signals are stored every 1.0 μs with a homemade MCS started with a trigger pulse supplied from the PEM.

The calcite polarizer is placed so that the direction of its polarization is parallel to the electric vector. The PEM is set so that when the voltage is not applied the direction of polarization is not rotated. The time-dependent intensity for the polarized photons perfectly perpendicular to the electric vector, $S(t)$, can be expressed by

$$S(t) = A |\sin at|, \quad (2a)$$

where t is the time (in the units of a microsecond) measured from the start of applying the voltage and a is a constant given by $a = \pi/(10 \mu\text{s})$. In the similar manner the time-dependent intensity of the fluorescence perfectly parallel to the electric vector of the exciting light is given by

$$S(t) = B - B |\sin at|. \quad (2b)$$

For the partially polarized photons the photon signal, $S(t)$, is expressed as

$$S(t) = C + D |\sin at| \quad (3)$$

and thus the ratio of the photon intensity perpendicular to that parallel to the electric vector, I_{\perp}/I_{\parallel} , is expressed as

$$\frac{I_{\perp}}{I_{\parallel}} = \frac{C+D}{C}. \quad (4)$$

These equations are valid for the photon intensity for an infinitely short time increment and a zero delay time for the trigger pulse applied to PEM. In the actual measurement accumulation of the photon signals was done for an increment of every 1.0 μs and the trigger pulse supplied from the PEM is nonzero. Therefore the photon count for the i th channel is fitted to a formula

$$S_i = C + D |\sin a(i+b)|, \quad (5)$$

where b is a phase shift in the units of a microsecond. The intensity ratio I_{\perp}/I_{\parallel} is given by the same equation as Eq. (4).

The resolution of the exciting light for absolute anisotropy measurement was $\Delta\lambda_{\text{ex}} = 0.50 \text{ nm}$. The gaseous pressure of XeF₂ was kept at 20 mTorr which ensures the collision-free condition during the XeF* excimer lifetime.

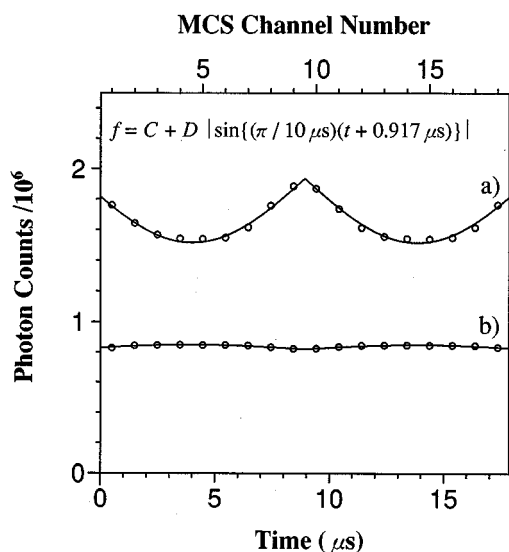


FIG. 2. PEM modulated spectra of photon signals observed for total XeF* emissions (○) and the least-square-fitted curves to a fitting function of $C + D |\sin\{\pi/10 \mu\text{s}(t + 0.917 \mu\text{s})\}|$. The channel width of the MCS was set at 1.0 μs . The spectra (a) and (b) were measured for exciting light wavelengths of 155.0 and 123.8 nm, respectively. The fitting parameters for spectrum (a) are $C = 1\,935\,710$ and $D = -420\,980$, and those for spectrum (b) are $C = 819\,610$ and $D = 28\,850$, respectively.

Figure 2 illustrates the typical PEM modulated spectra of the polarized fluorescence signals which oscillate with rotation of polarization direction for exciting light wavelengths of $\lambda_{\text{ex}} = 155.0$ and 123.8 nm. The least-squares fitting of the observed time spectrum to Eq. (5) gives us $b = 0.917 \mu\text{s}$. The fluorescence anisotropy values at $\lambda_{\text{ex}} = 155.0$ and 123.8 nm have been determined as $R = 0.084\,79 \pm 0.000\,17$ and $-0.011\,46 \pm 0.000\,28$, respectively.

2. Determination of fluorescence anisotropy using a dual-detector system

The fluorescence anisotropy of XeF* fragment emissions have been measured in a wide wavelength region of exciting light using a dual-detector system, as is shown in Fig. 1(b). The wavelength resolution of the exciting light was set at $\Delta\lambda_{\text{ex}} = 0.50 \text{ nm}$ to attain high enough photoemission intensity to keep the statistical error low within a short counting period. In some narrow wavelength region measurements were carried out at a resolution of $\Delta\lambda_{\text{ex}} = 0.10 \text{ nm}$. The pressure of gaseous XeF₂ was controlled to be 20 mTorr. In order to equalize the optical conditions for detection of emissions through two calcite polarizers whose directions are parallel and perpendicular to the electric vector of the exciting light, the photoelastic modulator used for the PEM-MCS experiment was removed for the present measurement.

Each set of polarizer-PMT detector emissions through a polarizer whose direction of polarization is *parallel* or *perpendicular* to the electric vector were counted by an Ortec photon counting system which is controlled by a microcomputer (NEC Model PC9801).

The emitted photons were accumulated using the dual-detector system for up to 100 s at each exciting light wavelength, λ_{ex} . The numbers of photons counted through the

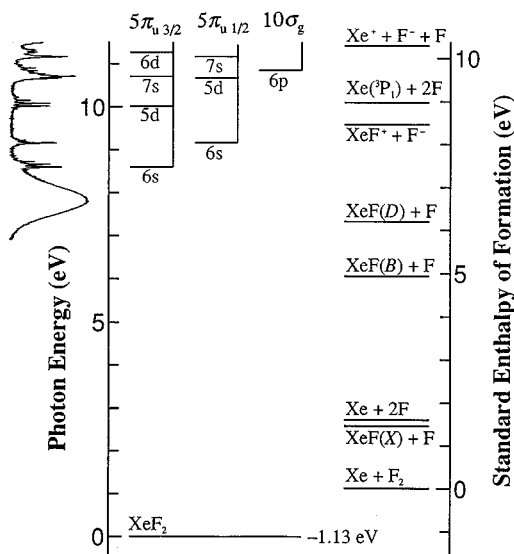


FIG. 3. Schematic diagram of the standard enthalpies of formation for the XeF₂ system and the photoexcitation energies for XeF₂. On the left a schematic absorption spectrum of XeF₂ is illustrated. Horizontal bars on the left correspond to the energy levels of the origins of the Rydberg bands. The standard enthalpies of formation are taken from Refs. 12, 15, 30, and 31.

polarizers parallel and perpendicular to the electric vector of the exciting light, N_{\parallel} and N_{\perp} , were obtained as a function of λ_{ex} , in a wide wavelength region. The disparity between the two detection systems has been corrected for by determining a scaling factor or correction factor, c , in

$$\frac{I_{\perp}}{I_{\parallel}} = c \frac{N_{\perp}}{N_{\parallel}} \quad (6)$$

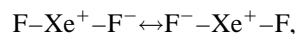
so that the standard deviation of the absolute R values [Eq. (1)] determined at six exciting wavelengths from those determined by the dual-detector system

$$R = \frac{1 - c(N_{\perp}/N_{\parallel})}{1 + 2c(N_{\perp}/N_{\parallel})} \quad (7)$$

becomes a minimum.

III. RESULTS AND DISCUSSION

The valence bond representation of the XeF₂ molecule may be expressed as the resonance hybrid of the two structures



which means that the Xe–F bonds have a half-ionic and half-covalent character. Figure 3 illustrates the energy levels of and the standard enthalpies of formation for the XeF₂ system^{12,15,30,31} along with a schematic absorption spectrum of gaseous XeF₂. Although the standard enthalpy of formation³⁰ of XeF₂ is only $\Delta H_f^0(\text{XeF}_2) = -1.13$ eV, it is a stable molecule since the standard enthalpy of dissociation for $\text{XeF}_2 \rightarrow \text{XeF}(X) + \text{F}$ is $\Delta H_f^0 = 2.61$ eV, which have been estimated from $\Delta H_f^0[\text{XeF}(X)] = 0.663$ eV, $\Delta H_f^0(\text{F}) = 0.824$ eV, and $\Delta H_f^0(\text{XeF}_2) = -1.13$ eV.³⁰ The standard enthalpies of dissociation of XeF₂ forming $\text{XeF}^*(B) + \text{F}$ and $\text{XeF}^*(D) + \text{F}$ products are 6.19 (200 nm) and 7.34 eV (169 nm), which

have been estimated from the ν_{00} energies for $B \rightarrow X$ and $D \rightarrow X$ transitions,³¹ i.e., 3.58 and 4.73 eV, respectively. The standard enthalpy of dissociation³⁰ of Xe–F in the ground ($X^2\Sigma_{1/2}^+$) state is determined as 0.160 eV which may be rather comparable to those of van der Waals bonds than chemical bonds.

The electronic configuration of XeF₂ in the ground electronic state is given^{10,11} in the following:

$$(8\sigma_g)^2(5\sigma_u)^2(9\sigma_g)^2(6\sigma_u)^2(4\pi_u)^4(3\pi_g)^4 \\ \times (10\sigma_g)^2(5\pi_u)^4(7\sigma_u)^0.$$

The lowest vacant orbital, $7\sigma_u$, which has an antibonding character consists mainly of $5p_z$ atomic orbitals (AOs) in Xe with a small contribution of $2s$ and $2p_z$ atomic orbitals in two F atoms. The highest occupied valence orbitals, $5\pi_u$, also have an antibonding character and consist of $5p_{x,y}$ AOs in Xe and $2p_{x,y}$ in two F atoms. Since the equilibrium Xe–F bond length in XeF₂ is long (197.4 pm),¹³ the mixing between the Xe p_x and F p_x orbitals or Xe p_y and F p_y orbitals is quite small and thus these orbitals are essentially of lone-pair electron character. The antibonding $10\sigma_g$ orbital consists of $5s$ in Xe, and $2s$ and $2p_z$ orbitals in two F atoms. The $3\pi_g$ and $4\pi_u$ consist of $2p_{x,y}$ in two F atoms and they are solely assigned as orbitals for lone-pair electrons of F atoms.

The ionization energies of the $5\pi_{u3/2}$, $5\pi_{u1/2}$, $10\sigma_g$, $3\pi_g$, $4\pi_{u3/2}$, and $4\pi_{u1/2}$ orbitals have been measured as 12.42, 12.89, 13.65, 14.35, 15.60, and 16.00 eV, respectively, using photoelectron spectroscopy.¹¹ The energy levels of the π_u orbitals split due to spin-orbit coupling.

The fundamental frequencies of XeF₂ have been determined by Bürger and his co-workers¹³ to be ν_1 (totally symmetric stretching)=519.05, ν_2 (bending)=212.38, and ν_3 (asymmetric stretching)=560.10 cm^{-1} . At 300 K the fraction

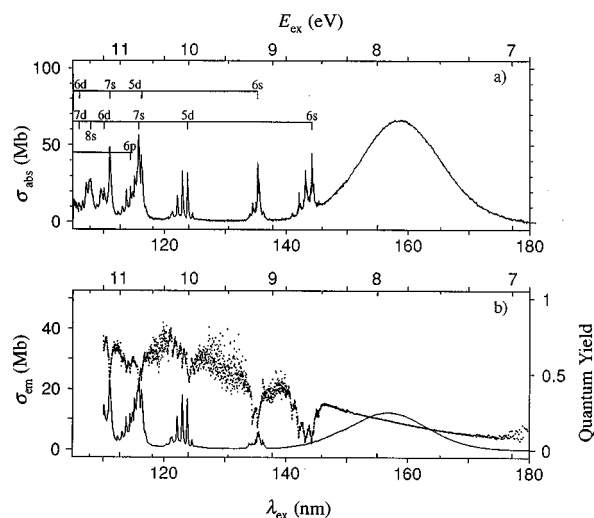


FIG. 4. (a) Absorption cross section (line), σ_{abs} , of XeF₂ plotted against the wavelength (bottom abscissa), λ_{ex} , and photon energy (top abscissa), E_{ex} , of the exciting light. (b) Photoemission cross section (line), σ_{em} , and the quantum yield (dots) for the total XeF* fragment formation in photodissociative excitation of the XeF₂ plotted against λ_{ex} (bottom abscissa) and E_{ex} (top abscissa). The spectral resolution of the exciting light was $\Delta\lambda_{\text{ex}} = 0.1$ nm.

TABLE I. Positions and assignments of the absorption and fluorescence excitation bands of XeF₂.

State	Assignment	$\lambda_{\text{ex}}(\text{nm})^{\text{a}}$	$\tilde{\nu}(\text{cm}^{-1})^{\text{b}}$	$\Delta\tilde{\nu}(\text{cm}^{-1})$	
$10\sigma_g \rightarrow 7\sigma_u$		158.00	63 291		
$5\pi_u \ 3/2 \rightarrow 6sR$	$1_1 2_1^1$	145.65	68 657	-667	
	1_1	145.38	68 785	-539	
	$1_1 2_2^2$	145.10	68 917	-407	
	$1_1 2_1^4$ or 2_2^2	144.84	69 041	-283	
	2_1^1	144.51	69 199	-125	
	0	144.25	69 324	0	
	2_2^2	144.00	69 444	120	
	2_1^4 or $1_1 2_2^2$	143.73	69 575	251	
	$1_1 2_1^1$	143.42	69 725	401	
	1_1^1	143.18	69 842	518	
	$1_1 2_2^2$	142.93	69 964	640	
	$1_1 2_1^4$ or $1_1 2_2^2$	142.65	70 102	778	
	$1_1 2_2^1$	142.37	70 240	916	
	1_1^2	142.11	70 368	1044	
	$1_1 2_2^2$	141.87	70 487	1163	
	$1_1 2_2^4$ or $1_1 3_2^2$	141.62	70 611	1287	
	$1_1 3_2^1$	141.32	70 761	1437	
	1_1^3	141.04	70 902	1578	
	$5\pi_u \ 1/2 \rightarrow 6sR$	$1_2 2_2^2$	137.54 ^c	72 706	-1182
		$1_2 2_1^1$	137.38 ^c	72 791	-1097
1_2		137.20 ^c	72 886	-1002	
$1_1 2_2^2$		136.55	73 233	-655	
$1_1 2_1^1$		136.40	73 314	-574	
1_1		136.23	73 405	-483	
2_1^1		135.57	73 763	-125	
0		135.34	73 888	0	
2_1^3		135.18	73 975	87	
2_2^2		135.01	74 069	181	
$1_1 2_2^2$		134.80	74 184	296	
$1_1 2_1^1$		134.69	74 245	357	
1_1^1		134.50	74 349	461	
$1_1 2_1^3$		134.17	74 532	644	
$1_1 2_2^2$		133.99	74 632	744	
1_1^2		133.65	74 822	934	
1_1^3		132.86	75 267	1379	
$5\pi_u \ 3/2 \rightarrow 5dR$	$1_1 2_1^1$	126.96 ^c	78 765	-619	
	1_1	126.82 ^c	78 852	-532	
	2_2	126.58 ^c	79 001	-383	
	2_2^2	126.33 ^c	79 158	-226	
	2_1^1	126.13 ^c	79 283	-101	
	0	125.97 ^c	79 384	0	
	2_2^2	125.73 ^c	79 536	152	
	$1_1 2_2^2$	125.46 ^c	79 707	323	
	$1_1 2_1^1$	125.28 ^c	79 821	437	
	1_1^1	125.10 ^c	79 936	552	
$5\pi_u \ 3/2 \rightarrow 5d_{\sigma}R$	1_1	124.61	80 252	-517	
	0	123.81	80 769	0	
	1_1^1	122.99	81 307	538	
	1_1^2	122.16	81 860	1091	
	1_1^3	121.34	82 413	1644	
	1_1^4	120.48	83 001	2232	
$5\pi_u \ 1/2 \rightarrow 5dR$...	119.54 ^c	83 654	-748	
	...	119.34 ^c	83 794	-608	
	$1_1 2_2^2$	119.14 ^c	83 935	-467	
	$1_1 2_1^1$	118.98 ^c	84 048	-354	
	1_1	118.84 ^c	84 147	-255	
	2_1^1	118.48 ^c	84 402	0	
	...	117.96 ^c	84 774	372	
	...	117.80 ^c	84 890	488	
...	117.48 ^c	85 121	719		
$5\pi_u \ 1/2 \rightarrow 5d_{\sigma}R$	1_1	116.96	85 499	-515	

TABLE I. (Continued.)

State	Assignment	$\lambda_{\text{ex}}(\text{nm})^{\text{a}}$	$\tilde{\nu}(\text{cm}^{-1})^{\text{b}}$	$\Delta\tilde{\nu}(\text{cm}^{-1})$	
	0	116.26	86 014	0	
	1_1^1	115.58	86 520	506	
	1_1^2	114.86	87 063	1049	
	1_1^3	114.18	87 581	1567	
$5\pi_u \ 3/2 \rightarrow 7sR$	1_1	116.38	85 925	-401	
	0	115.84	86 326	0	
	1_1^1	115.22	86 790	464	
	1_1^2	114.58	87 275	949	
	1_1^3	113.94	87 765	1439	
	1_1^4	113.19	88 347	2021	
$10\sigma_g \rightarrow 6p_{\sigma}R$	1_1	115.14	86 851	-539	
	0	114.43	87 390	0	
	1_1^1	113.78	87 889	499	
	1_1^2	113.13	88 394	1004	
	1_1^3	112.39	88 976	1586	
$5\pi_u \ 1/2 \rightarrow 7sR$	0	111.06	90 041	0	
	$5\pi_u \ 3/2 \rightarrow 6dR$	1_1	110.76	90 285	-542
		0	110.10	90 827	0
1_1^1		109.61	91 233	406	
$5\pi_u \ 3/2 \rightarrow 8sR$	1_1	108.24	92 387	-1560	
	0	107.68	92 868	0	
	1_1^1	107.18	93 301	2474	
	1_1^2	106.58	93 826	2999	

^aThe reproducibility of the wavelength reading is assessed to be ± 0.01 nm. The error of the absolute wavelength is estimated to be ± 0.05 nm.

^b $\tilde{\nu} = \lambda_{\text{ex}}^{-1}$.

^cObserved in the fluorescence excitation spectrum.

of molecules which are not vibrationally excited is estimated to be only 35%. Further 59% of XeF₂ molecules have at least one quantum of ν_2 vibrational energy. How the vibrational energy content in the XeF₂ molecule affects the probability of excimer formation is an interesting problem. Therefore one has to keep in mind that a relatively large fraction of the ambient gaseous XeF₂ molecules are vibrationally excited, which may influence apparent quantum yield for excimer formation, since some forbidden transitions can be allowed when some vibrational modes, especially the bending modes, are excited.

A. Absorption cross section and quantum yield for XeF* emission versus λ_{ex}

1. Absorption spectrum

The absorption spectrum of XeF₂ in the wavelength region of exciting light, $\lambda_{\text{ex}} = 105\text{--}180$ nm, is illustrated in Fig. 4(a) in which the absorption cross section (in Mb), σ_{abs} , is plotted against λ_{ex} . The absorption cross sections obtained in the present study agree fairly well with those which Black *et al.* have determined at 158 and 167 nm.⁶ The broad feature around 158 nm is assigned as the first allowed transition $10\sigma_g \rightarrow 7\sigma_u$. Several series of sharp bands in the shorter wavelength region than 160 nm are Rydberg transitions from the $5\pi_u \ 3/2$, $5\pi_u \ 1/2$, and $10\sigma_g$ orbitals whose band positions converge to the first (12.42 eV), second (12.89 eV), and third ionization energies (13.65 eV), respectively. The band

positions observed from the absorption and fluorescence excitation spectra are listed in Table I along with their assignments. Some of the bands which appear in the regions of 117–120, 125–128, and 137–138 nm were only observed in the fluorescence excitation spectrum.

2. Fluorescence excitation spectrum of the XeF* excimers

When XeF₂ is photoexcited, it is expected that the excited parent molecule XeF₂* does not emit fluorescence but undergoes fragmentation into two or three species. Possible nascent dissociation products forming diatomic fragments are XeF+F, Xe+F₂, and XeF⁺+F⁻. The electronic states available to the XeF molecule are $X^2\Sigma_{1/2}^+$, $A^2\Pi_{1/2,3/2}$, $B^2\Sigma_{1/2}^+$, $C^2\Pi_{3/2}$, and $D^2\Pi_{1/2}$. The XeF(X,A) fragments would be mostly dissociated to Xe+F as soon as formed, since the bond dissociation energy is too small to sustain a bound molecule. The XeF* excimers formed emit emissions at $\lambda_{\text{obs}} \approx 350$ nm for $B \rightarrow X$, ≈ 460 nm for $C \rightarrow A$, and ≈ 260 nm for $D \rightarrow X$ transition. The $C \rightarrow X$ and $D \rightarrow A$ transitions exhibit broad and very weak bands.^{2,14} The electronically excited F atom which emits strong resonance fluorescence in the vacuum UV region cannot be formed because of the low excitation energy used for the present experiment. The Xe+F₂ product would not be formed, since the two F atoms are far (~ 400 pm) apart in the ground state. The ion-pair dissociation channel, XeF⁺+F⁻, is only available when the excitation energy exceeds 9.59 eV (129.3 nm), but it is generally considered to be minor.¹⁵

The fluorescence excitation spectrum (FES) obtained by monitoring total emissions from XeF* excimers ($B \rightarrow X$, $C \rightarrow A$, and $D \rightarrow X$) is illustrated in Fig. 4(b) and the magnitude of the photoemission cross section, σ_{em} , is shown on the left ordinate. Figure 4(b) also shows the corresponding quantum yields (with dots). The quantum yield for total fluorescence is estimated as the ratio of the photoemission cross section relative to the absorption cross section at each λ_{ex} , assuming that emitting species are only XeF*(B, C, and D) excimers.

Although not shown, we have also measured partial photoemission cross sections for XeF* ($B \rightarrow X$) emission monitored using a filter (KL-53) with a maximum transmittance at 348.5 nm and a FWHM of 20.5 nm in the entire wavelength region of $\lambda_{\text{ex}} = 105$ –180 nm, where those of the total emissions are observed. As will be shown in the dispersed fluorescence spectrum, the emission detected at $\lambda_{\text{ex}} = 154.0$ nm is almost entirely ascribed to XeF*(B) fragments [see Fig. 5(e)]. As the excitation energy is raised, the ratio of a partial photoemission cross section relative to a total photoemission cross section is found to decrease but the ratio is larger than 0.5 even for $\lambda_{\text{ex}} < 120$ nm, despite the fact that XeF($D \rightarrow X$) emission is detected and XeF($B \rightarrow X$) emissions from vibrationally excited XeF* fragments are not transmitted through the filter used.

As is shown in Fig. 4(b), it is noted that the quantum yields for excimer formation are high in the entire wavelength region observed. In some region the quantum yields have been found to be close to unity. Probably the XeF₂ system is the one that most efficiently forms excimers in

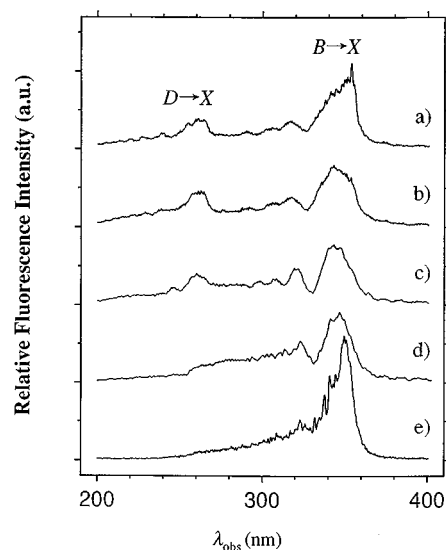


FIG. 5. Dispersed fluorescence spectra of XeF* formed at exciting light wavelength, λ_{ex} , of (a) 111.1, (b) 115.8, (c) 123.8, (d) 135.5, and (e) 154.0 nm in the observed fluorescence wavelength, λ_{obs} , region of 200–400 nm with a spectral resolution of $\Delta\lambda_{\text{obs}} = 1.2$ nm. The resolution of the exciting light was $\Delta\lambda_{\text{ex}} = 1.0$ nm.

photolysis and thus gives the highest quantum yield of all photodissociative excitation processes. Even the photodissociative excitation process of $\text{HCN} + h\nu \rightarrow \text{CN}^*(B) + \text{H}$ which is known to efficiently form excited fragments exhibits the highest quantum yield as high as 0.36.³² This high efficiency observed for the XeF* excimer formation may be due to a large bond energy for the XeF* molecule and the ionic nature of the Xe–F bonds even in the ground state of XeF₂.

Note that the quantum yield drastically decreases for Rydberg bands. In other words, the quantum yields are high in the region of weak absorbance (1–5 Mb) which may be called the background absorption region. The background absorption may be assigned to the transitions to intravalence excited states: the $10\sigma_g \rightarrow 7\sigma_u$ transition extended to the higher energy region, the weak but allowed $3\pi_g \rightarrow 7\sigma_u$ transition,¹⁶ and/or the forbidden $4\pi_u \rightarrow 7\sigma_u$ transition. These are discussed in detail in the following section.

3. Dispersed fluorescence spectra of XeF*

The dispersed fluorescence spectra of XeF* excimers are observed when XeF₂ is excited at (a) 111.1 ($5\pi_u 1/2 \rightarrow 7sR$), (b) 115.8 ($5\pi_u 3/2 \rightarrow 7sR$), (c) 123.8 ($5\pi_u 3/2 \rightarrow 5dR$), (d) 135.5 ($5\pi_u 1/2 \rightarrow 6sR$), and (e) 154.0 nm ($10\sigma_g \rightarrow 7\sigma_u$), as shown in Fig. 5. The $B \rightarrow X$ and $D \rightarrow X$ bands are observed near $\lambda_{\text{obs}} = 350$ and 260 nm, respectively. The $C \rightarrow A$ emission was observed around $\lambda_{\text{obs}} = 460$ nm but too weak to be easily identified.

It would be interesting to note that, when XeF₂ is excited at $\lambda_{\text{ex}} = 135.5$ and 154.0 nm, no conspicuous $D \rightarrow X$ bands are identified near $\lambda_{\text{obs}} = 260$ nm in the dispersed fluorescence spectra in Figs. 5(d) and 5(e). When XeF₂ is excited to Rydberg states higher than the $5\pi_u 1/2 \rightarrow 6sR$ state, i.e., for $\lambda_{\text{ex}} < 125$ nm, the XeF($D \rightarrow X$) emissions are observed. In fact, Black *et al.* have determined the quantum yield for

TABLE II. Fluorescence anisotropy values determined using the PEM-MCS system [*R* (PEM-MCS)] and the dual polarizer-detectors system [*R* (Dual)].

$\lambda_{\text{ex}}/\text{nm}$	<i>R</i> (PEM-MCS)	<i>R</i> (Dual)
123.8	-0.01146 ± 0.00028	-0.0100 ± 0.0037
130.0	0.02482 ± 0.00197	0.0063 ± 0.0089
135.5	0.00217 ± 0.00045	-0.0028 ± 0.0038
138.0	0.05547 ± 0.00261	0.0542 ± 0.0074
140.0	0.06911 ± 0.00250	0.0772 ± 0.0062
155.0	0.08479 ± 0.00017	0.0828 ± 0.0040

XeF*(*D*) formation to be 0.028 ± 0.005 at 155 nm as against for XeF*(*B*) formation to be 0.9 (+0.1, -0.2) at 158 nm.⁶ Bibinov and Vinogradov have determined that to be 5.9% relative to XeF*(*B*) formation.⁵

The onset for XeF*(*D*) formation has been found by Bibinov and Vinogradov to be about 167 nm which is close to the thermochemical limit of XeF*(*D*) formation (=169 nm).⁵ Monahan, Jones, and Rehn suggest that the $3\pi_g \rightarrow 7\sigma_u$ band excitation (>7.8 eV; 159 nm) of XeF₂ in a solid Kr matrix results in emission from the XeF*(*D*) state.¹⁷ Since dispersed fluorescence spectra have not been observed for the background region, one cannot conclude if the appreciable formation of XeF*(*D*) fragments occur or not as long as the excitation energy exceeds a certain energy or it depends on the excited state to which XeF₂ is brought. However one can point out that the *D*→*X* bands grow as the excitation energy is raised and are clearly observed for $\lambda_{\text{ex}} \leq 123.8$ nm where the excess energy for the XeF*(*D*) formation is 2.68 eV. As to the *B*→*X* bands, it is noted that the higher is the excitation energy, the broader the vibrational distribution becomes, which is inferred from the larger contributions of bound-free bands.

As is pointed out by Brashears, Setser, and Desmarreau,² the vibrational content of the XeF*(*B*) fragments formed at $\lambda_{\text{ex}} = 154.0$ nm in the $10\sigma_g \rightarrow 7\sigma_u$ band is rather low, which indicates that the energy of 1.97 eV available to the XeF*(*B*)+F product is mostly channeled to translational energy of the fragment pair and also to the rotational energy.

B. Fluorescence anisotropy

Table II summarizes the absolute fluorescence anisotropies, *R*, determined using the PEM-MCS system at six exciting wavelengths, λ_{ex} . In Fig. 6 they are plotted with open circles. In Fig. 6 are also plotted the normalized *R* values determined using the dual-detector system against λ_{ex} (with dots) in the wavelength region of $\lambda_{\text{ex}} = 105$ –180 nm along with the FES. It is noted that the *R* value strongly depends on the type of state to which the XeF₂ molecule is excited. The theoretical *R* values for the XeF* emission from photodissociative excitation of XeF₂ by linearly polarized light are listed in Table III.¹⁹ These values are evaluated for the XeF* fragments formed by direct dissociation. When the XeF₂ molecule is excited to a predissociative state, such as Rydberg states, the dissociating XeF₂* molecule may rotate during its lifetime. As a result, the memory of the spatial anisotropy created by polarized photoexcitation is partially lost, depending on the lifetime, and then the magnitude of the *R*

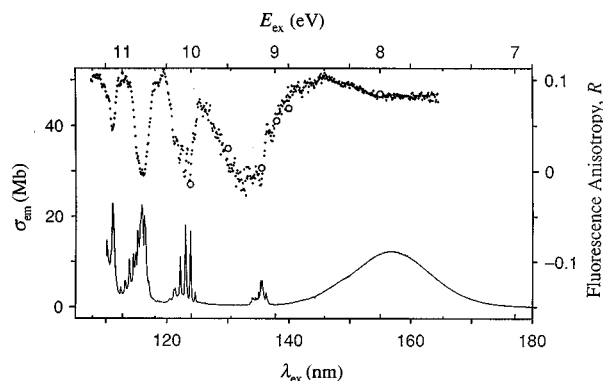


FIG. 6. Fluorescence anisotropy (dots), *R*, obtained for total XeF* emission, whose ordinate is indicated on the right against λ_{ex} (bottom abscissa) and E_{ex} (top abscissa) along with the photoemission cross section (solid line), σ_{em} , whose ordinate is indicated on the left. The spectral resolutions of the exciting light for the anisotropy and fluorescence excitation spectra were 0.50 and 0.10 nm, respectively. The absolute *R* values (○) determined using the PEM-MCS system are also plotted for comparison.

value measured will be less than the theoretical limit listed in Table III. If more processes contribute to the fragment emission, the observed *R* value is the averaged *R* value of weights of their cross sections for all processes.

When XeF₂ is excited through the $10\sigma_g \rightarrow 7\sigma_u$ intravalence transition, the fluorescence anisotropy is found to be about 0.085. On the other hand, in the $5\pi_u$ series of the Rydberg bands converging to the first and second ionization energies, the *R* value decreases and for some bands it becomes even negative.

The wave functions of both XeF($X^2\Sigma_{1/2}^+$) and XeF*($B^2\Sigma_{1/2}^+$) molecules are symmetric along the C_∞ bond axis. The ground state wave function of XeF* ($X^2\Sigma_{1/2}^+$) is correlated to the ground state Xe(1S_0) atom plus the F($^2P_{3/2}$) atom at infinite nuclear separation and the half occupied $2p_z$ orbital in F is directed along the molecular axis. The electronic structure of the excited XeF*($B^2\Sigma_{1/2}^+$) molecule has an ion-pair or charge-transfer character of $\text{Xe}^+(^2P_{3/2})\text{-F}^-(^1S_0)$ in which a $5p_z$ electron in Xe is transferred to the F atom and is correlated to $\text{Xe}^+(^2P_{3/2})\text{+F}^-(^1S_0)$ at infinite internuclear separation. Therefore the XeF(*B*→*X*) fluorescence transition moment, μ_{em} , is parallel to the C_∞ bond axis. In a similar manner the excited XeF*($D^2\Pi_{1/2}$) molecule has an ion-pair

TABLE III. Theoretical fluorescence anisotropy values of XeF* excimers formed in the direct photodissociation of XeF₂.

$\mu_{\text{em}} \parallel (\text{Xe-F})^*$ axis	$\mu_{\text{em}} \perp (\text{Xe-F})^*$ axis	
	<i>P</i> , <i>R</i> branch	<i>Q</i> branch
Bent parent molecule		
$\mu_{\text{abs}} \parallel (\text{F-Xe-F})^*$ plane	1/10	-1/5
$\mu_{\text{abs}} \perp (\text{F-Xe-F})^*$ plane	-1/5	2/5
Linear parent molecule		
$\mu_{\text{abs}} \parallel (\text{F-Xe-F})^*$ axis	1/10	-1/5
$\mu_{\text{abs}} \perp (\text{F-Xe-F})^*$ axis		
<i>P</i> , <i>R</i> branch	1/10	-1/5
<i>Q</i> branch	-1/5	2/5

character of Xe⁺(²P_{1/2})-F⁻(¹S₀) in which a 5p_z electron in Xe has transferred to the F atom leaving a spin-orbit excited Xe⁺(²P_{1/2}) ion. The C²Π_{3/2} excited state of the XeF* excimer has also a charge transfer character and is correlated to Xe⁺(²P_{3/2})+F⁻(¹S₀) at infinite internuclear separation.

The parent XeF₂ molecule has a D_{∞h} symmetry. When the transition moment of photoabsorption of XeF₂ is parallel to the molecular C_∞ axis, it is in the plane of rotation of the XeF* fragment for high rotational quantum numbers. When the transition moment of photoabsorption, μ_{abs} , is perpendicular to the C_∞ axis, it can be either in the plane of rotation of the fragment or make some arbitrary angle to the plane. We now assume that the dissociating photoexcited XeF₂* molecule is bent and thus the XeF* fragment rotates in the plane of bent molecule. If the absorption transition moment is perpendicular to the molecular plane, then the *R* value for XeF(*B*→*X*) emission should be negative. In contrast if this transition moment is in the molecular plane, the *R* value will be positive. Further if the excited XeF₂* molecule does not dissociate immediately after photoexcitation, it will rotate around the angular momentum of the excited molecule during the lifetime of XeF₂* and thus the absolute value of *R* will decrease.

Note that the emissions are mostly due to XeF*(*B*) fragments. Since the transition moments assigned to 10σ_g→7σ_u and 10σ_g→nρ_σ*R* transitions are parallel to the molecular axis and that assigned to 5π_u→ns*R* or nd_σ*R* is perpendicular to the molecular axis, it is expected that the former transitions give positive anisotropy values and the latter gives negative or low anisotropy values. For the 10σ_g→6ρ_σ*R* bands, the *R* value does not drop from the *R* values of the background absorption. The present results of fluorescence anisotropy measurements support the above-mentioned assignments, that is, the 10σ_g→7σ_u and 10σ_g→6ρ_σ*R* transitions are parallel and the 5π_u→ns*R* or nd_σ*R* transitions are perpendicular to the molecular C_∞ axis. In the following section detailed reasoning will be provided. The *R* values observed for the perpendicular transitions do not approach the limiting value, -0.2, probably due to (i) a large contribution of the intravalence transitions which give rise to the background absorption, (ii) low quantum yields for excimer formation for the Rydberg transition, (iii) some contribution of a Rydberg transition whose transition moment is in the molecular plane (see Table III), and finally (iv) a contribution of nonzero lifetime of the excited state.

C. Discussion of individual bands

1. 10σ_g→7σ_u band

a. Quantum yields. As is shown in Fig. 4(a) a strong broad feature is observed in the region 140–180 nm in the absorption and fluorescence excitation spectra, except for the sharp Rydberg bands appearing in the region 141–146 nm. This broad feature has been assigned to an allowed intravalence transition: 10σ_g→7σ_u. Vibrational progressions are not observed for this band, since XeF₂ is excited to a repulsive, dissociative state, ... (10σ_g)¹(5π_u)⁴(7σ_u)¹. It is interesting to note that the quantum yield for XeF* total emission increases with photon energy for this intravalence band from

~10% to 30%, except for the region of Rydberg bands. Black *et al.* have obtained the quantum yields for excimer fluorescence to be about 90% at λ_{ex}=145 and 172 nm.⁶ They seem to be too high since our values are found to be 26% and 10% at 145 and 172 nm, respectively, and the values of Bibinov *et al.* are around 34%. If the quantum yield in this wavelength region of about 90% were to be true, the quantum yield of 74% at 110.5 nm would be scaled to be 260%. As is shown in the dispersed fluorescence spectrum [see Fig. 5(e)] and from the partial photoemission cross sections mentioned above which were measured using a bandpass filter to detect XeF(*B*→*X*) emission, most of the emissions in this region are due to XeF(*B*→*X*).

It is inferred that the 10σ_g→7σ_u(Σ_u⁺) state is correlated with the direct dissociative channel leading to XeF*(*B*) and XeF(*X*) because they are of the same symmetry. Since the XeF(*X*) state is only weakly bound and dissociated into Xe+F as soon as formed, the nonradiative channel will produce Xe+2F.

b. Fluorescence anisotropy. As is shown in Fig. 6, the *R* values observed in this region are very high (≈0.085). It compares well with the theoretical limit of the fluorescence anisotropy for the direct dissociative excitation after parallel transition of the parent molecule, i.e., *R*=1/10 (see Table III). Therefore these results present a typical example confirming that if a linear molecule photoexcited with a transition moment parallel to the molecular C_∞ axis directly dissociates forming an excited fragment whose transition moment of emission is along the molecular axis, then the fluorescence anisotropy should be nearly 1/10. The fact that the observed anisotropy (*R*≈0.085) is smaller than the theoretical limit must be due to the contribution of XeF*(*B*) fragments with low rotational quantum numbers. Since the parent molecule is linear and the fragment emission is parallel to the molecular axis, the sources of rotational excitation of the XeF*(*B*) fragments are the thermal rotational energy and bending vibrational motions of the parent molecule.

2. 3π_g→7σ_u (allowed valence) and 4π_u→7σ_u (forbidden valence) transitions

The fluorescence anisotropy spectrum shown in Fig. 6 reveals a decrease in *R* value in the wavelength region 125–140 nm, while the quantum yield for excimer formation keeps rising except for the Rydberg bands as the photon energy is raised. One may have to call for some other excited states than the ones called for to assign the absorption spectrum, such as the allowed intravalence (10σ_g→7σ_u) and Rydberg transitions. Therefore to explain the lowering of the *R* value observed, allowed valence 3π_g→7σ_u and the forbidden valence 4π_u→7σ_u transitions are called for though they do not show conspicuous bands in the absorption spectrum. The 3π_g→7σ_u transition is dipole allowed and has a parallel transition moment along the molecular C_∞ axis. The 4π_u→7σ_u transition can be allowed if combined with asymmetric stretching or bending vibrations. The transition moments induced by the asymmetric stretching and bending vibrations are perpendicular and parallel to the molecular C_∞ axis, respectively. The decrease in the *R* value at around 130

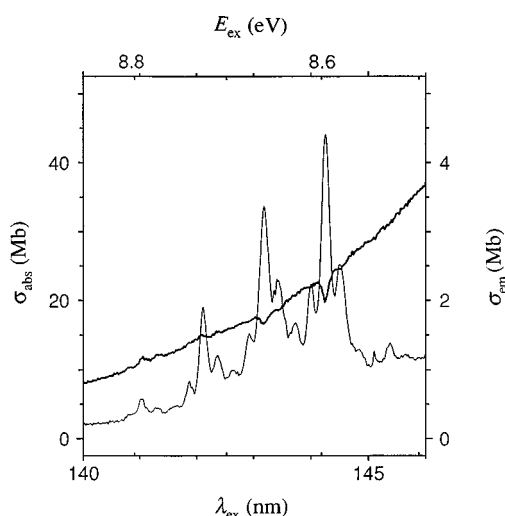


FIG. 7. Absorption cross section (thin line), σ_{abs} , and photoemission cross section (bold line), σ_{em} , against λ_{ex} (bottom abscissa) and E_{ex} (top abscissa) in the expanded region of $\lambda_{\text{ex}}=140\text{--}146$ nm. The spectral resolution was $\Delta\lambda_{\text{ex}}=0.10$ nm. Fluorescence dips are observed in the $5\pi_{u\ 3/2}\rightarrow 6sR$ bands. The assignments of vibronic bands are summarized in Table I.

nm where no conspicuous absorption band is observed, may be explained by invoking these intravalence transitions.

The strong broad $10\sigma_g\rightarrow 7\sigma_u$ absorption band has a maximum at 158 nm (7.84 eV). If it is assumed that a shift in the excitation energy for any other bands is estimated using the difference in the ionization energies determined by the photoelectron spectrum of XeF₂, then the $3\pi_g\rightarrow 7\sigma_u$ excitation would appear at 8.54 eV (145.2 nm). In a similar manner the excitation energies for $4\pi_{u\ 3/2}\rightarrow 7\sigma_u$ and $4\pi_{u\ 1/2}\rightarrow 7\sigma_u$ would appear at 9.79 eV (126.7 nm) and 10.19 eV (121.7 nm), respectively. Considering the facts that the potential energy surface for the antibonding state $7\sigma_u$ is of a repulsive nature, the $10\sigma_g\rightarrow 7\sigma_u$ absorption band is very broad, and the excitation energy may shift with the change in the structure, it may be likely that the bands giving rise to these transitions shift to and appear in the region from 125 to 140 nm.

3. $5\pi_{u\ 3/2}\rightarrow 6sR$ bands

a. Fluorescence dips. Figure 7 illustrates the absorption and fluorescence excitation spectra and the quantum yields. In the previous section, we have noted that the quantum yield decreases for the Rydberg bands, which means that the excited XeF₂^{*} molecule in the Rydberg states are preferentially dissociated to the product channels leading to nonradiative fragments. A most interesting and distinct observation is made for the series of $5\pi_{u\ 3/2}\rightarrow 6sR$ bands around 143 nm concerning the efficient quenching of the excited state. The absorption spectrum of XeF₂ (thin line) and XeF₂^{*} total fluorescence excitation spectrum (bold line) are illustrated in Fig. 7 in the expanded region from 140 to 146 nm. Note that no peaks are observed in the fluorescence excitation spectrum in spite of intense absorption bands (30–40 Mb) observed.

These findings would be explained by the obvious reason that this Rydberg state is quite efficiently channeled into nonradiative dissociation products, Xe+2F. If one carefully

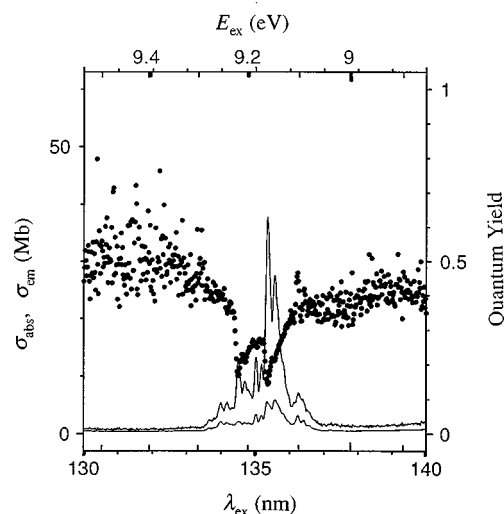


FIG. 8. Absorption cross section (upper curve), σ_{abs} , and photoemission cross section (lower curve), σ_{em} , and quantum yield (dots) against λ_{ex} and E_{ex} in the expanded region of 130–140 nm. The spectral resolution was $\Delta\lambda_{\text{ex}}=0.10$ nm. The assignments of vibronic bands for the $5\pi_{u\ 1/2}\rightarrow 6sR$ transitions are summarized in Table I.

examines the fluorescence excitation spectrum, even dips are found at 143.18 and 144.25 nm, whereas weak positive bands are observed at 141.04 and 142.11 nm. It seems that the fluorescence bands which are negative at lower energies tend to become positive as the exciting light energy is increased. A similar phenomenon has been observed for the strong Rydberg absorption band in I₂,³³ in which system however the changeover of the fluorescence intensity from a negative to a positive value has not been observed.

b. Dark states. The occurrence of the fluorescence dips indicate that the probability of relaxation from its excited state to the nonradiative channels is unity and the XeF₂^{*} molecules photoexcited via the $10\sigma_g\rightarrow 7\sigma_u$ intravalence transitions at the same excitation energies as the $5\pi_{u\ 3/2}\rightarrow 6sR$ Rydberg bands tend to be relaxed into the same nonradiative dissociation channels as the Rydberg state. This indicates that this intravalence state can easily interact with the Rydberg states. The XeF₂^{*} molecule in this Rydberg state is bent since the vibrational progressions of the bending (ν_2) mode are observed in the absorption spectrum, while the $10\sigma_g\rightarrow 7\sigma_u$ intravalence state is linear. It would be possible that, if the parent molecules whose bending vibrations are thermally excited are photoexcited via $10\sigma_g\rightarrow 7\sigma_u$ intravalence transitions, they might undergo intramolecular energy transfer to a dark state via the $5\pi_{u\ 3/2}\rightarrow 6sR$ Rydberg states.

It is speculated that other intravalence states than the $10\sigma_g\rightarrow 7\sigma_u$ state may contribute to the nonradiative channel and may be considered as a candidate for the dark state. The $5\pi_u\rightarrow 7\sigma_u$ transition can be allowed and thus has the same character as the $10\sigma_g\rightarrow 7\sigma_u$ transition, if the molecule is bent in the excited state and the transition is accompanied by a bending vibration.

4. $5\pi_{u\ 1/2}\rightarrow 6sR$ bands

a. ν_2 quanta dependence of the quantum yield. Figure 8 illustrates the absorption and fluorescence excitation spectra

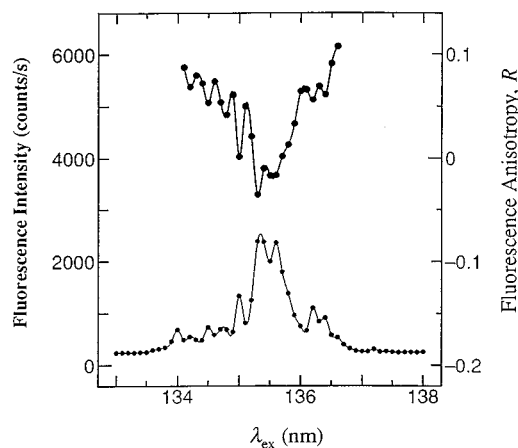


FIG. 9. Fluorescence anisotropy (upper dots and curve), R , whose ordinate is indicated on the right along with the fluorescence intensity (lower dots and curve) in the wavelength region of 133–138 nm. The fluorescence intensity is the averaged count rates, $I_{\parallel} + 2I_{\perp}$, for parallel and perpendicular emission intensities, I_{\parallel} and I_{\perp} , which were used to evaluate R values. The lines are drawn to guide the eyes. The spectral resolution was $\Delta\lambda_{\text{ex}}=0.10$ nm. The R values have been determined so that they agree well with those shown in Fig. 6.

and quantum yields in the wavelength region of $\lambda_{\text{ex}}=130$ –140 nm. The molecule is bent in this Rydberg state since the bending vibrational progressions are observed in the absorption spectrum. Judging from the vibrational progressions in the absorption spectrum this state must have essentially the same structure as the $5\pi_u 1/2 \rightarrow 6sR$ except for the slight differences in the vibrational frequencies and the bending angle: the progressions of totally symmetric stretching vibration (ν_1) are not found for high excitation levels and the vibrational energy spacings are different from those of the $5\pi_u 1/2 \rightarrow 6sR$ state. Note that the quantum yield for XeF* excimer formation varies with increasing the bending (ν_2) quantum number. Even if the stretching vibration is excited at 134.50 nm (1^1 transition), the quantum yield has not increased at all. Therefore, one can conclude that bending vibration in the excited XeF*₂ molecule promotes excimer formation, but stretching vibration does not. This fact may be explained in terms of the enhancement of interaction of this state with the intravalence background states via the bending vibrations.

b. Fluorescence anisotropy. Figure 9 illustrates the photofragment fluorescence anisotropy along with the fluorescence intensity plotted against λ_{ex} measured for a resolution of exciting light $\Delta\lambda_{\text{ex}}=0.10$ nm around the $5\pi_u 1/2 \rightarrow 6sR$ bands. Since the photon count rates were low, the standard deviation is about 0.01. Since this transition is perpendicular to the molecular C_{∞} axis, the R value decreases at the peaks of the FES. The structure of this excited state is bent. Therefore, the direction of the absorption transition moment is either in the plane of the bent molecular plane or parallel to it. Since the transitions to both directions can contribute to the anisotropy value, the R values determined for these bands turn out to be approximately zero.

5. $5\pi_u \rightarrow 5d_{\sigma}R$ bands

a. Excited state structure and quantum yields. Figure 10

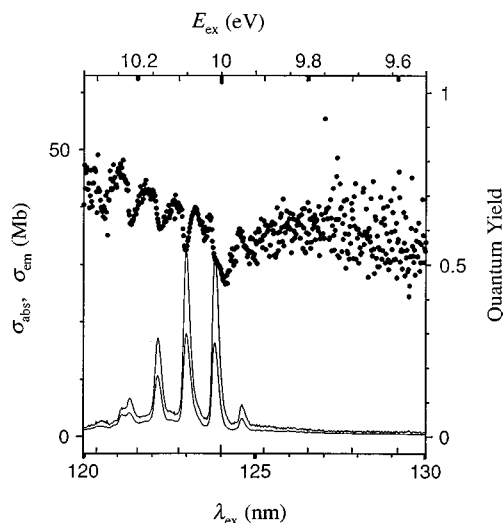


FIG. 10. Absorption cross section (upper curve), σ_{abs} , and photoemission cross section (lower curve), σ_{em} , and quantum yield (dots) against λ_{ex} and E_{ex} in the expanded region of 120–130 nm. The spectral resolution was $\Delta\lambda_{\text{ex}}=0.10$ nm. The assignments of vibronic bands for the strong $5\pi_u 3/2 \rightarrow 5d_{\sigma}R$ transitions are summarized in Table I.

illustrates the absorption and fluorescence excitation spectra and quantum yields in the wavelength region of $\lambda_{\text{ex}}=120$ –130 nm. The progressions of the bending (ν_2) vibration are not observed in the $5\pi_u 3/2 \rightarrow 5dR$ band, from which it follows that the molecular structure is linear and that the force field determining the fundamental frequency of bending vibration, ν_2 , is very comparable to that of the ground state. The quantum yields are smaller than those for the background absorption and decrease only a little for the bands of this Rydberg transition. Compared with the $5\pi_u 3/2, 1/2 \rightarrow 6sR$ bands the decrease is rather minor.

b. Fluorescence anisotropy. Figure 11 illustrates the R values plotted against λ_{ex} measured for a resolution of exciting light of $\Delta\lambda_{\text{ex}}=0.10$ nm along with the FES around the $5\pi_u 3/2 \rightarrow 5dR$ bands. The R value decreases for these bands, but the minima positions of R do not agree with the positions of the band maxima for FES. From the results of fluorescence anisotropies this transition is concluded to be perpendicular to the C_{∞} axis. Therefore this Rydberg orbital has either δ or σ symmetry. These bands have been assigned to $5d_{\delta}R$ by Nielsen and Schwarz.⁷ As will be mentioned in the next section, since the two weak Rydberg series have been observed at the excitation energies lower than the bands assigned as $5\pi_u 3/2, 1/2 \rightarrow 5dR$, we would like to assign these bands to $5\pi_u 3/2, 1/2 \rightarrow 5d_{\sigma}R$ transitions.

The finding that the minima positions of R do not agree with the positions of the band maxima for FES is remarkable. This phenomenon may be due to the contributions of different states which are not resolved with the resolution of the exciting light used. They may be either an excited state combined with a bending vibration or the states giving rise to P , Q , or R branch transitions; three branch transitions are possible since this excited state has a linear structure. If P , Q , and R branches were well resolved, the P and R branch bands would appear on the lower energy side and the Q branch band would appear on the higher energy side. From

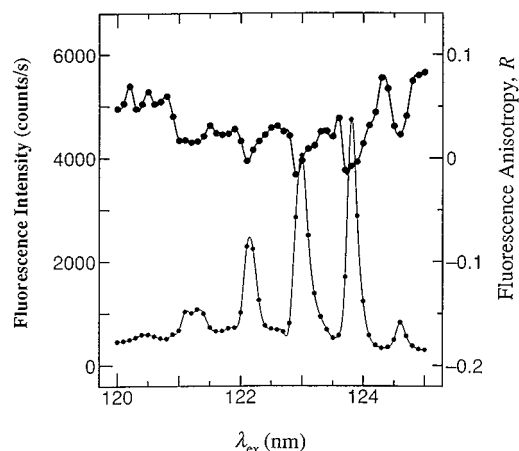


FIG. 11. Fluorescence anisotropy (upper dots and curve), R , whose ordinate is indicated on the right along with the fluorescence intensity (lower dots and curve) in the wavelength region of 120–125 nm. The fluorescence intensity is the averaged count rates, $I_{\parallel} + 2I_{\perp}$, for parallel and perpendicular emission intensities, I_{\parallel} and I_{\perp} , which were used to evaluate R values. The lines are drawn to guide the eyes. The spectral resolution was $\Delta\lambda_{\text{ex}} = 0.10$ nm. The R values have been determined so that they agree well with those shown in Fig. 6.

Table III the R value is expected to be low for the Q branch and higher for the P and R branch bands, which is observed in the fluorescence anisotropy spectrum as is seen in Fig. 11.

6. Newly observed weak progressions in FES

Figures 12 and 13 illustrate the fluorescence excitation spectra in the wavelength regions of $\lambda_{\text{ex}} = 124.75$ – 127.25 nm and 117.25–119.75 nm, respectively. One can find weak progressions of the bending ν_2 vibration in these spectra. It was not possible to assign these bands as hot bands of the strong $5\pi_u$ and $5\pi_u$ transitions, since the energy separation of the stretching vibrations would be made too large. The $5d$ Rydberg orbitals are classified as σ_g , π_g , and δ_g and the quantum defect for each orbital can be different. At present these weak bands are assigned to the $5d_{\pi}$ or $5d_{\delta}$ Rydberg bands with different symmetries from that for the strong Rydberg bands observed in the absorption spectrum.

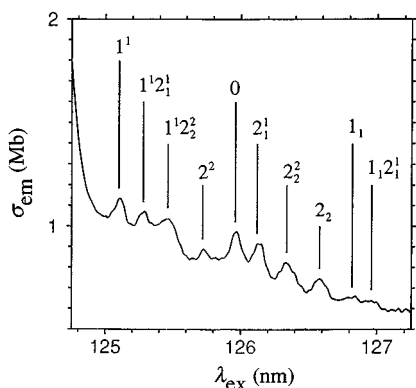


FIG. 12. Photoemission cross section, σ_{em} , of XeF₂ against λ_{ex} in the expanded region of $\lambda_{\text{ex}} = 124.75$ – 127.25 nm. The assignments of the vibronic bands for the weak $5\pi_u$ transitions are indicated.

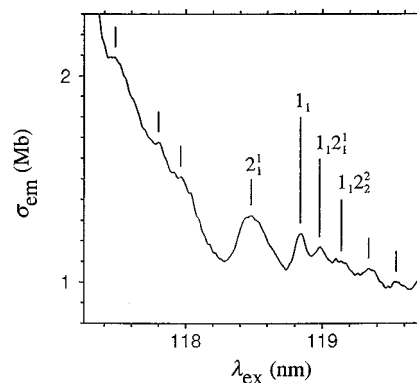


FIG. 13. Photoemission cross section, σ_{em} , of XeF₂ against λ_{ex} in the expanded region of $\lambda_{\text{ex}} = 117.25$ – 119.75 nm. The assignments of the vibronic bands for the weak $5\pi_u$ transitions are indicated.

7. $10\sigma_g \rightarrow 6pR$, $5\pi_u$ and other Rydberg bands up to 106 nm

a. Quantum yields. Figure 14 illustrates the absorption and fluorescence excitation spectra and quantum yields in the wavelength region of $\lambda_{\text{ex}} = 105$ – 120 nm. The quantum yield is determined to be 0.74 for the exciting light, $\lambda_{\text{ex}} = 110.5$ nm. Bibinov and Vinogradov report that the quantum yield for XeF* formation for the exciting light of $\lambda_{\text{ex}} = 116$ nm is larger than 0.70, whereas our measurement gives a value of 0.50 at this wavelength. High quantum yields for XeF* excimer formation have been observed for the broad background absorption bands; the maximum quantum yield is recorded to be around 0.80 at $\lambda_{\text{ex}} \approx 120$ nm, although the noise level is high. Since the absolute emission intensity is low, the dispersed fluorescence spectra have not been observed for the background absorption bands. Therefore it is not known which is the major emissive product when the molecule is excited by the background absorption.

b. Fluorescence anisotropy. Figure 15 illustrates the R values against λ_{ex} determined for a wavelength resolution of

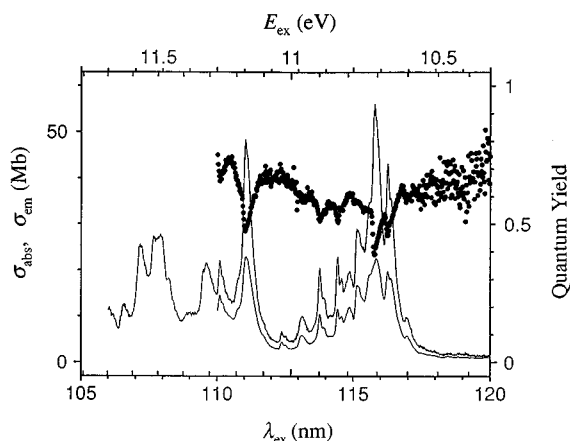


FIG. 14. Absorption cross section (upper curve), σ_{abs} , and photoemission cross section (lower curve), σ_{em} , and quantum yield (dots) against λ_{ex} and E_{ex} in the expanded region of 106–120 nm. The spectral resolution was $\Delta\lambda_{\text{ex}} = 0.10$ nm. The assignments of vibronic bands for the $5\pi_u$ transitions are summarized in Table I.

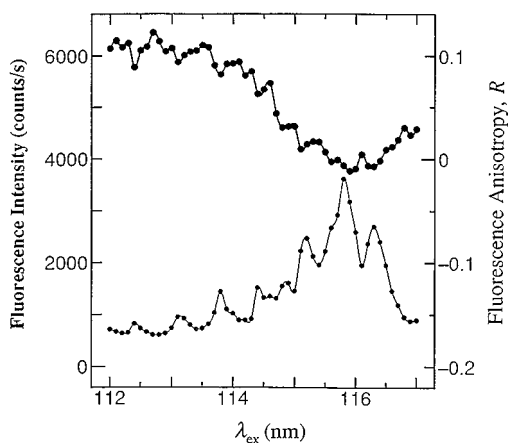


FIG. 15. Fluorescence anisotropy (upper dots and curve), R , whose ordinate is indicated on the right along with the fluorescence intensity (lower dots and curve) in the wavelength region of 112–117 nm. The fluorescence intensity is the averaged count rates, $I_{\parallel} + 2I_{\perp}$, for parallel and perpendicular emission intensities, I_{\parallel} and I_{\perp} , which were used to evaluate R values. The lines are drawn to guide the eyes. The spectral resolution was $\Delta\lambda_{\text{ex}}=0.10$ nm. The R values have been determined so that they agree well with those shown in Fig. 6.

$\Delta\lambda_{\text{ex}}=0.10$ nm along with the fluorescence excitation spectrum in the region 112–117 nm. For the $10\sigma_g \rightarrow 6pR$ bands, the R value does not decrease from those for the background absorption, from which results it has been concluded that the symmetry of the $6p$ Rydberg orbital is of σ type.

D. Dissociation mechanism

The energy level diagram and the heats of formation for the XeF₂ in Fig. 3 show that the XeF(B,D)+F channels can be accessed energetically at excitation wavelengths shorter than 200 and 169 nm, respectively. Since the vibrational energy content of the XeF*(B) fragments formed at $\lambda_{\text{ex}}=154.0$ nm, as measured from the dispersed fluorescence, is small, a large fraction of the excess energy (1.99 eV) may be channeled into translational motion of the XeF*(B)+F fragments pair. It may be natural to consider that the XeF*(B) excimers with an axial symmetric property are predominately formed in the $10\sigma_g \rightarrow 7\sigma_u$ excitation, whose transition moment is parallel to the F–Xe–F molecular C_{∞} axis. Even upon excitation at 135.5 nm however XeF($D \rightarrow X$) emission was observed to be only a few percent of the total excimer emission, but conspicuous XeF($D \rightarrow X$) emission was observed at $\lambda_{\text{ex}}=123.8$ nm. This means that an excess energy of 1.81 eV is not enough for formation of appreciable amount of XeF*(D) but 2.68 eV has turned out to be enough. Both of the Rydberg transitions are assigned to be perpendicular to the molecular C_{∞} axis. From the viewpoints of the symmetry of the transition moment as well as the energetics, both of the Rydberg transitions can form XeF*(D) excimers. Thus a large amount of excess energy may be needed to efficiently form XeF*(D) excimers.

State-selective dissociation has been found by Lee and his co-workers in the photolysis of CH₂BrI, especially when the excited states are antibonding repulsive states.³⁴ As the

excitation energy is raised, intramolecular electronic-energy transfer tends to occur rapidly, since nonadiabatic coupling between adjacent states becomes larger.^{34–36}

Whether the product distribution among different excimer states depends upon the character of the excited state or only on the excess energy available in the product is an important question. Since the dispersed fluorescence spectra have not been observed for the background absorption which spans essentially the whole region of excitation energy above 140 nm studied, we cannot say if a XeF*(D) excimer can be easily formed by photoexcitation in the background absorption. Therefore it would be worthwhile to measure dispersed fluorescence spectra in the background absorption region, although the intensity level is low.

As is already mentioned, with increasing the excitation energy, the quantum yield increases for the background absorption. This trend can be applied even for Rydberg transitions, as long as they are compared only among these transitions, although quantum yields drop from the level of the background absorption. Why the quantum yields range only from 10% to 30% for the $10\sigma_g \rightarrow 7\sigma_u$ broadband is an unanswered question. It might be useful to point out that a large fraction of XeF₂ molecules are vibrationally excited. Further from the expanded spectra of the Rydberg transitions one may conclude that the larger the vibrational energy in the excited XeF₂ molecule, the higher the quantum yield for excimer formation. In order to know whether the quantum yield for excimer formation strongly depends on the internal state of the electronically excited XeF₂ molecule, one may need to carry out jet cooled experiments as well as higher resolution experiments than the present one, using vacuum UV lasers.

One can consider that, in the photon energy region of the present study, whenever a XeF* excimer is not formed the photoexcited XeF*₂ molecule is automatically channeled into one of the dark states which end up forming nonradiative products, i.e., Xe+2F. The dark states may not be optically allowed. The question is then “Can the $5\pi_u \rightarrow 3/2 \rightarrow 6sR$ Rydberg state be a dark state?” We do not consider it to be one, since very weak excimer fluorescence was detected when XeF₂ is excited at 141.04 and 142.11 nm, whereas no emission was observed for all other bands. We consider that the dark states are not bound but are repulsive states which exclusively lead the molecule to the Xe+2F product. The $5\pi_u \rightarrow 3/2 \rightarrow 6sR$ Rydberg state can only be very efficiently relaxed or redistributed to a dark state. At photoexcitation energies higher than the 7 eV intramolecular redistribution rate among available states seems to be fairly high but it seems that a statistical behavior cannot be applied; if all of the energetically available states, including electronic states, are equally taken into consideration, a considerable increase in quantum yield for excimer formation with excitation energy to almost unity, which has been observed, can never be explained. Therefore in a simple molecule, such as XeF₂, as the photoexcitation energy is raised, the tendency of keeping an electronic energy persists and thus the quantum yield for XeF* excimer formation increases with increasing excitation energy, even for some of the high lying Rydberg states. Therefore, one can consider that an intramolecular redistribu-

tion rate to the dark state(s) is strongly dependent on the individual vibronic state as well as the molecular geometry of the excited state.

The Rydberg excitations of the $5\pi_u$ electrons induce the removal of an essentially lone-pair electron from the central Xe atom to one of the Rydberg orbitals. Since the Xe–F bond has a half ion-pair character in the electronic ground state, the removal of one electron from the Xe atom is not necessarily a favorable process to form an XeF* excimer which also has an ion-pair character. Thus if a Xe–F bonding electron is excited to an antibonding orbital, a Xe–F bond rupture is induced and then the quantum yield for excimer formation would be higher. Therefore, from simple-minded considerations intravalence transitions favor excimer formation but disfavor Rydberg transitions. However, one may have to call for a bottleneck intermediate state which effectively leads the excited system to ion-pair state formation. The higher the excitation energy the wider may be the opening of the bottleneck leading to ion-pair product formation.

At present we do not know what kind of state the bottleneck state is. In explaining the observed results including absorption spectra, FES, quantum yields for excimer formation, and fluorescence anisotropy values we have so far considered only singlet states or optically accessible states. We may have to invoke triplet states as dark states to which energy transfer occurs very fast. It would be very helpful if potential energy surface calculations for the singlet states as well as the triplet states of XeF₂ are made to the energy levels up to about 12 eV.

ACKNOWLEDGMENTS

The authors thank Professor N. Kosugi for fruitful discussions on the potential energy surfaces of XeF₂ in their excited states. Useful comments given by the referee are appreciated.

- ¹E. G. Wilson, J. Jortner, and S. A. Rice, *J. Am. Chem. Soc.* **85**, 813 (1963).
- ²H. C. Brashears, Jr., D. W. Setser, and D. Desmarteau, *Chem. Phys. Lett.* **48**, 84 (1977).
- ³J. F. Bott, R. F. Heidner, J. S. Holloway, and J. B. Koffend, *Chem. Phys.* **148**, 411 (1990).
- ⁴N. K. Bibinov, I. P. Vinogradov, and D. B. Stavrovskii, *Kvantovaya Elektron.* **8**, 1945 (1981).
- ⁵N. K. Bibinov and I. P. Vinogradov, *Opt. Spektrosk.* **57**, 355 (1984).
- ⁶G. Black, R. L. Scharpless, D. C. Lorents, D. L. Huestis, R. A. Gutcheck,

- T. D. Bonifield, D. A. Helms, and G. K. Walters, *J. Chem. Phys.* **75**, 4840 (1981).
- ⁷U. Nielsen and W. H. E. Schwarz, *Chem. Phys.* **13**, 195 (1976).
- ⁸G. W. Loge and J. R. Wiesenfeld, *Chem. Phys. Lett.* **78**, 32 (1981).
- ⁹G. W. Loge and J. R. Wiesenfeld, *J. Chem. Phys.* **75**, 2795 (1981).
- ¹⁰G. L. Gutev and A. E. Smoljar, *Chem. Phys.* **56**, 189 (1981).
- ¹¹C. R. Brundle, M. B. Robin, and G. R. Jones, *J. Chem. Phys.* **52**, 3383 (1970).
- ¹²J. E. Velazco, J. H. Kolts, D. W. Setser, and J. A. Coxon, *Chem. Phys. Lett.* **46**, 99 (1977).
- ¹³H. Bürger, R. Kuna, S. Ma, J. Breidung, and W. Thiel, *J. Chem. Phys.* **101**, 1 (1994).
- ¹⁴H. Helm, D. L. Huestis, M. J. Dyer, and D. C. Lorents, *J. Chem. Phys.* **79**, 3220 (1983).
- ¹⁵J. Berkowitz, W. A. Chupka, P. M. Guyon, J. H. Holloway, and R. Spohr, *J. Phys. Chem.* **75**, 1461 (1971).
- ¹⁶H. Basch, J. W. Moscovitz, C. Hollister, and D. Hankin, *J. Chem. Phys.* **55**, 1922 (1971).
- ¹⁷K. M. Monahan, V. O. Jones, and V. Rehn, *J. Chem. Phys.* **71**, 2360 (1979).
- ¹⁸J. P. Simons, *J. Phys. Chem.* **91**, 5378 (1987).
- ¹⁹T. Nagata, T. Kondow, K. Kuchitsu, G. W. Loge, and R. N. Zare, *Mol. Phys.* **50**, 49 (1983).
- ²⁰G. A. Chamberlain and J. P. Simons, *Chem. Phys. Lett.* **32**, 355 (1975).
- ²¹G. A. Chamberlain and J. P. Simons, *J. Chem. Soc. Faraday II* **71**, 2043 (1975).
- ²²M. T. Macpherson and J. P. Simons, *Chem. Phys. Lett.* **51**, 261 (1977).
- ²³M. T. Macpherson and J. P. Simons, *J. Chem. Soc. Faraday II* **74**, 1965 (1978).
- ²⁴M. T. Macpherson and J. P. Simons, *J. Chem. Soc. Faraday II* **75**, 1572 (1979).
- ²⁵J. A. Guest, M. A. O'Halloran, and R. N. Zare, *Chem. Phys. Lett.* **103**, 261 (1984).
- ²⁶K. Kanda, S. Katsumata, T. Nagata, Y. Ozaki, T. Kondow, K. Kuchitsu, A. Hiraya, and K. Shobatake, *Chem. Phys.* **175**, 399 (1993).
- ²⁷M. Kono, A. Hiraya, K. Tabayashi, K. Shobatake, T. Ibuki, and T. Nakao (unpublished results).
- ²⁸K. Shobatake, A. Hiraya, K. Tabayashi, and T. Ibuki, in *Vacuum Ultraviolet Photoionization and Photodissociation of Molecules and Clusters*, edited by C. Y. Ng (World Scientific, Singapore, 1991), p. 503.
- ²⁹L. C. Lee, L. Oren, E. Phillips, and D. L. Judge, *J. Phys. B* **11**, 47 (1978).
- ³⁰S. G. Lias, J. E. Bartmess, J. F. Liebman, J. L. Holmes, R. D. Levin, and W. G. Mallard, *J. Phys. Chem. Ref. Data* **17** (1988).
- ³¹K. P. Huber and G. Herzberg, *Constants of Diatomic Molecules* (Van Nostrand Reinhold, New York, 1979).
- ³²L. C. Lee, *J. Chem. Phys.* **72**, 6414 (1980).
- ³³A. Hiraya, K. Shobatake, R. J. Donovan, and A. Hopkirk, *J. Chem. Phys.* **88**, 52 (1988).
- ³⁴L. J. Butler, E. J. Hints, S. F. Shane, and Y. T. Lee, *J. Chem. Phys.* **86**, 2051 (1987).
- ³⁵E. Jensen, J. S. Keller, G. C. G. Waschewsky, J. E. Stevens, R. L. Graham, K. F. Freed, and L. J. Butler, *J. Chem. Phys.* **98**, 2882 (1993).
- ³⁶P. W. Kash, G. C. G. Waschewsky, and L. J. Butler, *J. Chem. Phys.* **99**, 4479 (1993).